Electronic Supplementary Material (ESI) for Inorganic Chemistry Frontiers.
This journal is © the Partner Organisations 2023

SUPPORTING INFORMATION

Observation of Long-Lived Phosphorescence in Au(I) Complexes Bearing Chromophoric (N-Heterocyclic Carbene) Ligands

Evan P. Van Orman,[a] Steven M. Wolf,[e,f] Zheng Yung,[c] Ethan D. Holt,[c] Kimberly de La Harpe,[d] Matthias Zeller,[b] Tod A. Grusenmeyer[e] and Thomas G. Gray[a,*]

Contents

Instrumentation. Ground-state UV/vis absorption spectra were measured using a Perkin-Elmer spectrophotometer. Luminescence spectra were obtained using a Horiba PTI QM-400 fluorometer. Ground-state absorption spectra of **IDPA-AuBr** and **IBTF-AuBr** in toluene is shown in Figure S1.

Absolute Fluorescence Quantum Yield Measurements. Absolute fluorescence quantum yield values were determined using a Horiba PTI QM-400 fluorometer outfitted with an integrating sphere. A detailed discussion of collecting and determining absolute quantum yields using an integrating sphere is described elsewhere.[1] Briefly, aerated samples of **IDPA-AuBr** and **IBTF-AuBr** were prepared in toluene to have an absorbance of 0.1 at the excitation wavelength of 340 nm. The excitation intensity was determined by placing a blank toluene sample inside the integrating sphere, setting the excitation bandwidth to 1 nm, and adjusting the emission slit until 1 million counts registered at the detector, which corresponded to a slit width of 0.75 nm. The emission spectra were collected under identical conditions with the samples and blank toluene placed inside the integrating sphere. All spectra were collected from 320 nm – 600 nm using a step size of 0.3 nm, a 0.5 s dwell time, and an average of 3 scans for each trial. Each quantum yield measurement was collected in triplicate. Absolute fluorescence quantum yield values (Φ_f) were obtained using Equation S1.[1]

$$\Phi_f = \frac{\int \lambda/hc \left[I_{em}^{sample}(\lambda) - I_{em}^{blank}(\lambda)\right] d\lambda}{\int \lambda/hc \left[I_{ex}^{blank}(\lambda) - I_{ex}^{sample}(\lambda)\right] d\lambda} \quad \text{(S1)}$$

The number of photons absorbed by the sample was determined by integrating the excitation signal (I_{ex}^{sample}) from 320 to 360 nm for **IBTF-AuBr** and 320 to 367 nm for **IDPA-AuBr** and subtracting it from the excitation signal from the blank toluene (I_{ex}^{blank}) over the same range. The number of photons emitted by the sample was determined by integrating the fluorescence signal (I_{em}^{sample}) from 360 to 560 nm for **IBTF-AuBr** and 368 to 575 nm for **IDPA-AuBr** and subtracting the integrated fluorescence signal from blank toluene over the same range (I_{em}^{blank}) from it. Absolute fluorescence quantum yield measurements are reported in Table 1. Sample self-absorption was negligible ($a < 0.03$) and not included in the reported absolute fluorescence quantum yield values. Data used to determine the absolute fluorescence quantum yield values for **IDPA-AuBr** and **IBTF-AuBr** is shown in Figure S2.

Phosphorescence Quantum Yields using Absolute Fluorescence Quantum Yields. Quenching of the excited triplet state by oxygen requires deaeration via freeze-pump-thaw (FPT) of the sample in order to observe and accurately quantify phosphorescence. An absolute quantum yield measurement for phosphorescence is not possible because the FPT cell does not fit within the integrating sphere of the Horiba PTI QM-400 fluorometer. Instead, relative phosphorescence quantum yield measurements were obtained using the absolute fluorescence quantum yield measurements described previously.[2] **IBTF-AuBr** and **IDPA-AuBr** samples were prepared in toluene to have an absorbance of 0.1 at the excitation wavelength of 340 nm. Samples underwent three freeze-pump-thaw cycles to a final cell pressure of 3 mTorr. Luminescence spectra were measured and scaled to match the fluorescence spectrum of the aerated samples. Due to overlap between the fluorescence and phosphorescence signals in **IBTF-AuBr** and **IDPA-AuBr**, the integrated fluorescence intensity (Int_{FL}) was obtained by integrating the fluorescence signal of the aerated samples. The integrated phosphorescence intensity (Int_{PHOS}) was obtained by integrating the luminescence spectra and subtracting the integrated fluorescence intensity. The relative phosphorescence quantum yield values (Φ_{PHOS}) were obtained using the following Equation S2.[2]

$$\Phi_{PHOS} = \frac{Int_{PHOS}}{Int_{FL}} \Phi_{FL} \quad \text{S2}$$

Data used to determine the relative phosphorescence quantum yield values for **IDPA-AuBr** and **IBTF-AuBr** is shown in Figure S3 and the values reported in Table 1.

Intersystem Crossing Quantum Yields using Photosensitized Singlet Oxygen. A method for determining photosensitized singlet oxygen quantum yields has been previously reported.[3–5] Aerated samples of **IBTF-AuBr**, **IDPA-AuBr**, and **phenazine**, the reference standard, were prepared in toluene to have an absorbance of 0.1 at the excitation wavelength of 372 nm. NIR luminescence spectra were measured using an Edinburgh Instruments FLS1000 spectrometer. A picosecond pulsed diode laser (372.4 ± 0.8 nm, 65 ps pulse width) was paired with an adjustable neutral density filter to attenuate the intensity before the sample. The emission signal was collected at 90° relative to the excitation source and passed through a single Czerny-Turner emission monochromator (325 nm focal length, 1800 grooves/mm grating optimized for 500 nm, 830 grooves/nm grating optimized for 1200 nm, 1.7 nm/mm dispersion) before collection with a Hamamatsu R5509-72 photomultiplier in a nitrogen-flow cooled housing (Operating temperature: −80 ℃). Back-to-back singlet oxygen phosphorescence spectra from 1240 – 1320 nm were collected for all samples under identical conditions. An emission correction factor was applied to the spectra to correct for wavelength dependence of the emission light path. The photosensitized singlet oxygen quantum yield of a sample using a reference standard was determined using equation S3.[5]

$$\Phi_{\Delta,x} = \Phi_{\Delta,std}\left(\frac{F_x}{F_{std}}\right)\left(\frac{f_{std(\lambda_{ex,std})}}{f_s(lambda_{ex},x)}\right)\left(\frac{\eta_x^2}{\eta_{std}^2}\right) \quad \text{S3}$$

$\Phi_{\Delta,x}$ is the photosensitized singlet oxygen quantum yield of the unknown and $\Phi_{\Delta,std}$ is the photosensitized singlet oxygen quantum yield of the reference standard, $\Phi_{\Delta,std} = 0.88$ for phenazine.[4] F_x and F_{std} are the integrated luminescence intensity values obtained for the unknown and reference standard. $f_x(\lambda_{ex,x})$ and $f_{std}(\lambda_{ex,std})$ represent the fraction of light absorbed by the unknown and reference standard. η^2_x and η^2_{std} are the indices of refraction for the solvents used to collect the luminescence spectra of the unknown and the reference, which are the same in these experiments. This method provides a lower limit for the intersystem quantum yield (ISC) quantum yield for each sample. The data used to determine the relative ISC quantum yield values for **IDPA-AuBr** and **IBTF-AuBr** is shown in Figure S4 and reported in Table 1.

Fluorescence and Phosphorescence Lifetime Measurements. Fluorescence and phosphorescence lifetime measurements were obtained using an Edinburgh Instruments FLS1000 spectrometer. Samples were prepared to have an optical density of approximately 0.1 at the excitation wavelength of 372 nm. The samples were excited with a picosecond pulsed diode laser (372.4±0.8 nm, 65 ps pulse width) which was paired with an adjustable neutral density filter to attenuate the intensity before the sample. The emission signal was collected at 90° relative to the excitation source and passed through a single Czerny-Turner emission monochromator (325 nm focal length, 1800 grooves/mm grating optimized for 500 nm, 830 grooves/nm grating optimized for 1200 nm, 1.7 nm/mm dispersion) before collection with a high-speed PMT detector (Hamamatsu H10720-01). The IRF FWHM for the system is 194 ps. Fluorescence lifetimes measurements were obtained using time-correlated single photon counting (TCSPC) with the excitation diode laser operating at a repetition rate of 20 MHz. Emission was collected at the wavelength of the fluorescence maximum with a bandwidth of 2.0 nm. Lifetimes were determined by fitting the decays to a single exponential function using a reconvolution fitting routine within the Fluoracle software. Fluorescence lifetime measurements were run in triplicate with the average reported in Table 1. For phosphorescence lifetime measurements, samples were deaerated via three freeze-pump thaw cycles to a final cell pressure of 3 mTorr. Measurements were obtained using multi-channel scaling with the excitation diode laser set at a repetition rate of 125 Hz. Emission was collected at the wavelength of the second phosphorescence maximum (to minimize contributions from fluorescence) with a 17.33 nm

bandwidth. Lifetimes were determined by tail-fitting the decay signals to a single exponential within the Fluoracle software. Phosphorescence lifetime measurements were run in triplicate with the average reported in Table 1. The data used to determine the fluorescence and phosphorescence lifetimes for **IDPA-AuBr** and **IBTF-AuBr** is shown in Figures S5 and S6, respectively.

Rate Constant Determinations. The rate constant for radiative, k_r, non-radiative, k_{nr}, and intersystem crossing, k_{ISC}, were determined from equations S4-S6, and reported in Table 1.

$$\tau_F = \frac{1}{k_r + k_{nr} + k_{ISC}} \quad \text{S4}$$

$$\Phi_F = \frac{k_r}{k_r + k_{nr} + k_{ISC}} \quad \text{S5}$$

$$\Phi_{ISC} = \frac{k_{ISC}}{k_r + k_{nr} + k_{ISC}} \quad \text{S6}$$

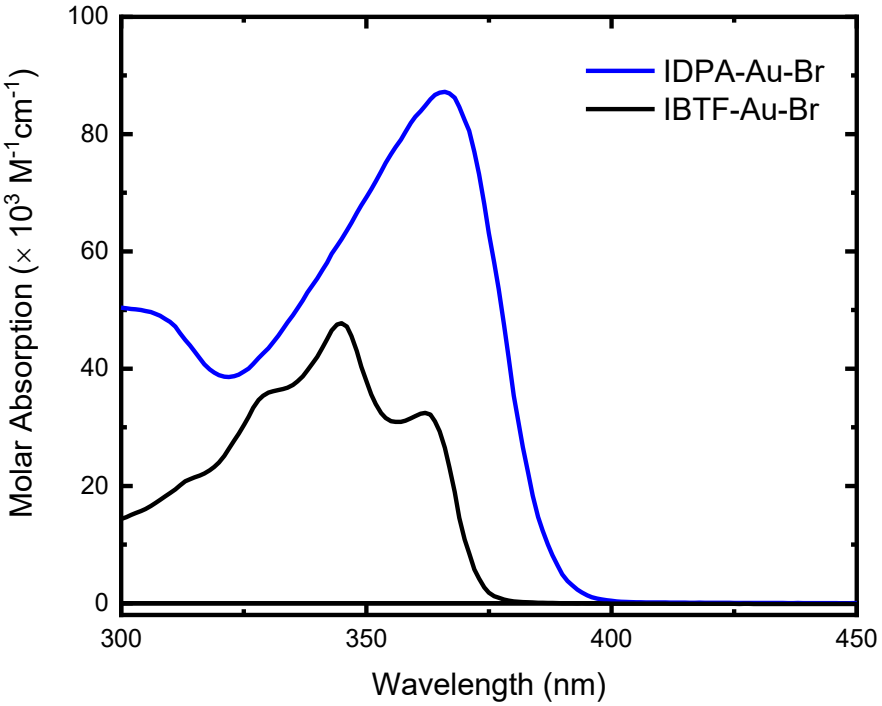

Figure S1: Ground-state absoprtion spectra of **IDPA-AuBr** and **IBTF-AuBr** in units of molar absorptivity versus wavelength in toluene.

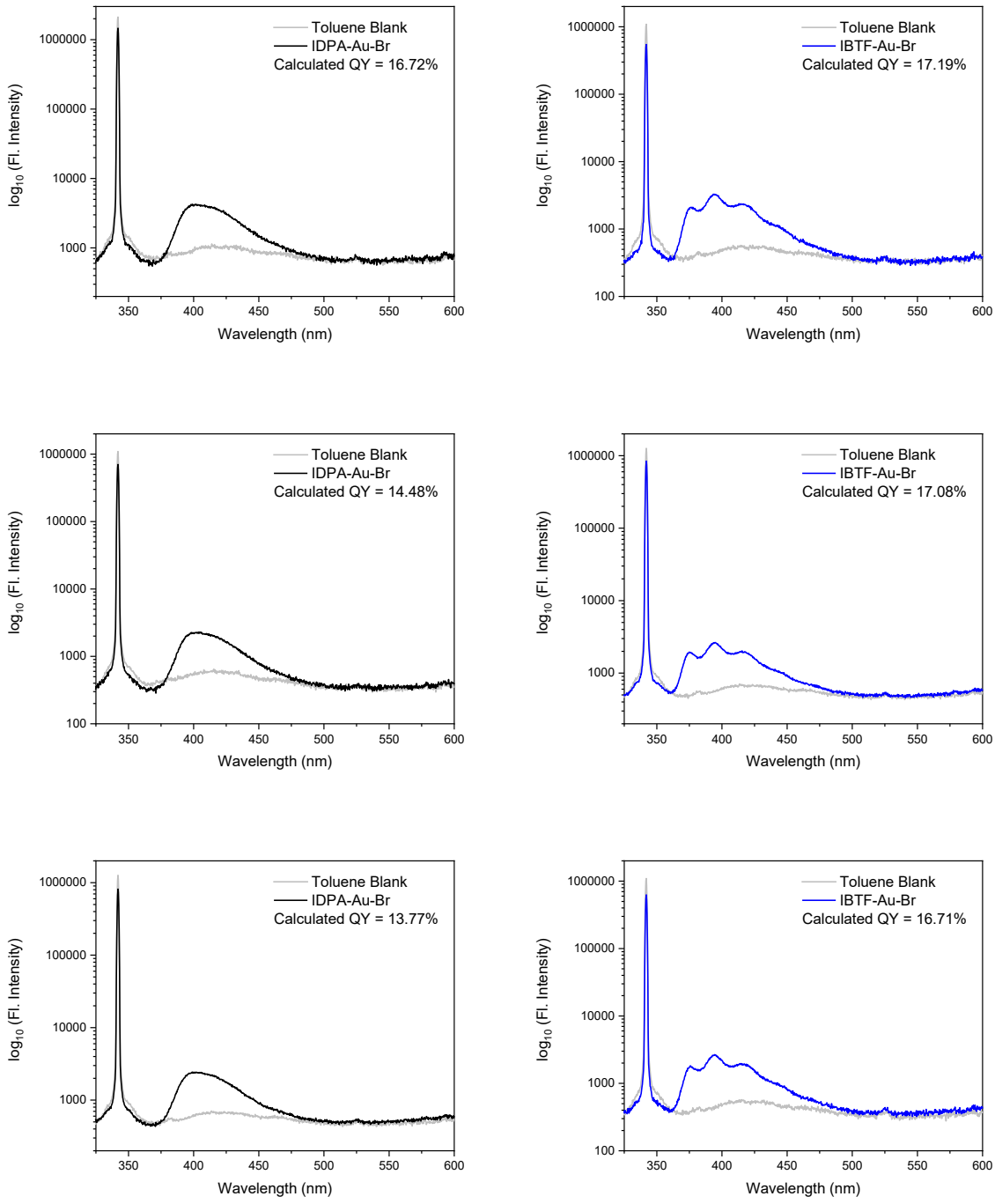

Figure S2. Absolute fluorescence quantum yields (left) of **IDPA-AuBr** and (right) of **IBTF-AuBr** in toluene. Quantum yields were measured in triplicate using an integrating sphere with the average reported in Table 1.

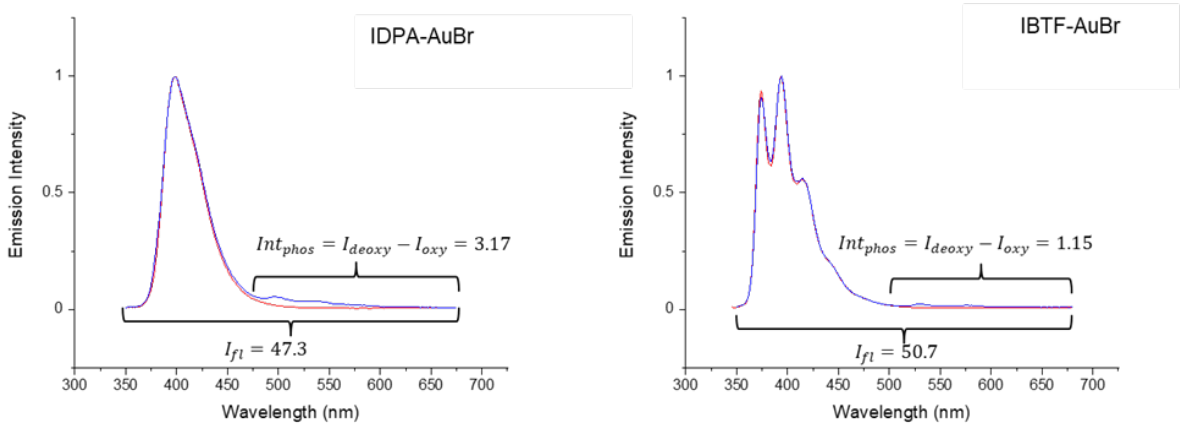

Figure S3. Luminescence spectra of **IDPA-AuBr** (left) and **IBTF-AuBr** (right) under oxygenated (red) and deoxygenated (blue) conditions showing integrated areas used to measure relative phosphorescence quantum yields.

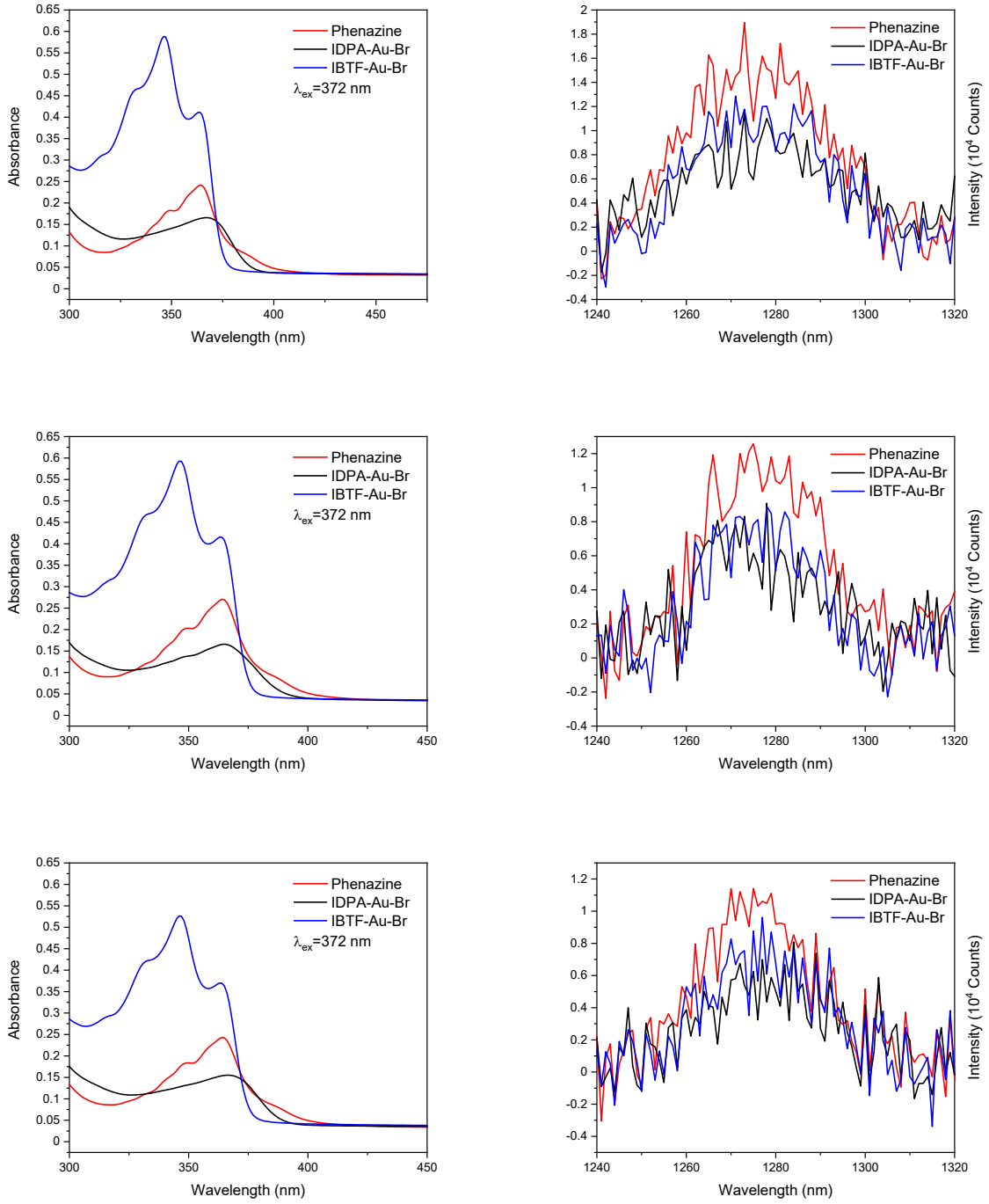

Figure S4. Absorption (left) and singlet oxygen phosphorescence (right) of **phenazine**, **IDPA-AuBr** and **IBTF-AuBr**. All samples were prepared in toluene, and the average of triplet-state quantum yields from the three trials reported in Table 1.

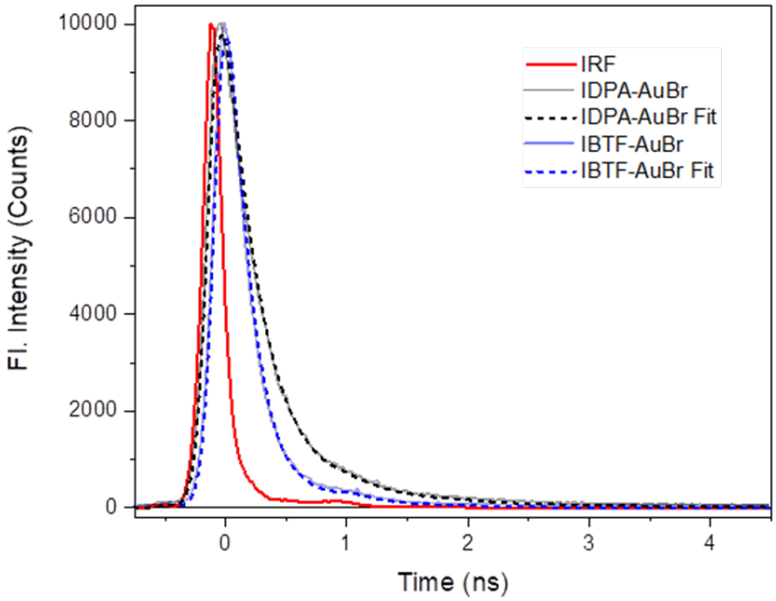

Figure S5. Fluorescence lifetime decays of **IDPA-AuBr** (ex. 372nm; em. 397 nm) and **IBTF-AuBr** (ex. 372 nm; em. 394 nm) collected in toluene. The average fluorescence lifetime from three measurements is reported in Table 1.

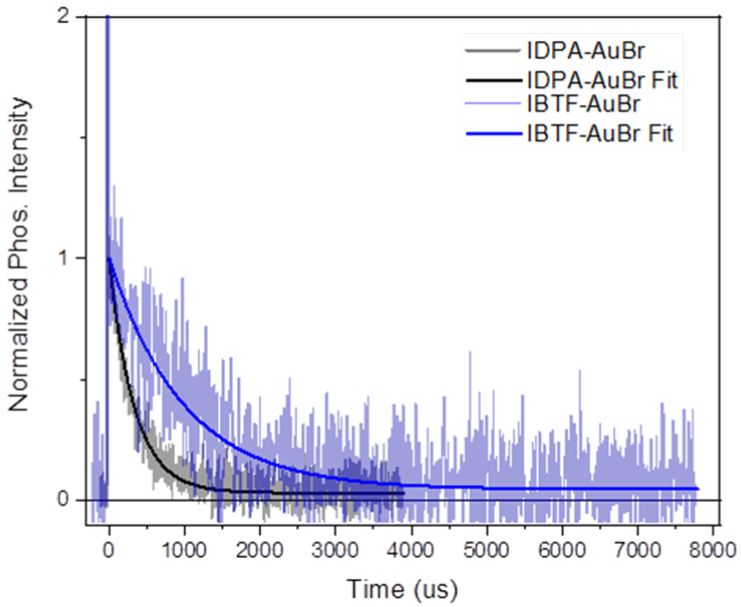

Figure S6. Phosphorescence lifetime decays of **IDPA-AuBr** (ex. 372 nm; em. 537 nm) and **IBTF-AuBr** (ex. 372 nm; em. 575 nm) collected in deoxygenated toluene. Decays are normalized to the maximum of the

phosphorescence signal with the fluorescence signal off scale. The fluorescence signal is 19 and 83 times greater than the phosphorescence signal for **IDPA-AuBr** and **IBTF-AuBr**, respectively. The average phosphorescence lifetime from three measurements is reported in Table 1.

Synthesis, ^{1}H NMR, and Mass Spectrometry

All ligand synthesis was done under atmospheric conditions unless stated otherwise. All organometallic reactions were done with exclusion of air under argon. Reagents and solvents were purchased from TCI, MilliporeSigma, and Fisher Scientific; all were used as received. (IPr)AuCl was prepared according to published methods.[6] Diphenylamine- and benzothiazolyl-substituted fluorenes were prepared as described by Tan and co-workers.[7] Reactions involving air- or moisture-sensitive compounds were performed with standard Schlenk and vacuum line techniques in flame- or oven-dried glassware. ^{1}H nuclear magnetic resonance (NMR) spectra were collected on a Bruker-500 Ascend Advanced III HD NMR spectrometer operating at 500.24 MHz. All NMR experiments were run at millimolar concentration. ^{1}H chemical shifts are reported in parts per million (δ) relative to tetramethylsilane (0 ppm) and are referenced to residual solvent in $CDCl_3$ (7.26 ppm) with integration and multiplicity (s = singlet, d = doublet, t = triplet, q = quartet, dd = doublet of doublets, dt = doublet of triplets, td = triplet of doublets, ddd = doublet of doublet of doublets, and m = multiplet). Electrospray impact (ESI) ultrahigh resolution mass spectrometry data were collected at the Campus Chemical Instrument Center (CCIC) at The Ohio State University.

1-(7-(benzo[d]thiazol-2-yl)-9,9-diethyl-9H-fluoren-2-yl)-3-benzyl-1H-imidazol-3-ium (IBTF)

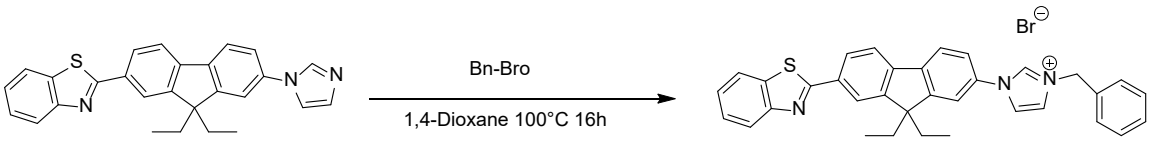

Scheme S1: Synthetic route for the attachment of the benzyl moiety to the imidazole of BTF-Im.

To a 50-mL round-bottom flask equipped with a Vigreux column were added BTF-Im (426 mg, 1.00 mmol) and benzylbromide (0.218 mL, 1.84 mmol) with 10 mL 1,4-dioxane. The mixture was stirred at 100 °C for 16 h. The reaction mixture was cooled to room temperature, whereupon 50 mL deionized water was added with formation of an off-white precipitate. The suspension was filtered and washed with water (5 × 10 mL) and redissolved in dichloromethane. This solution was dried with $MgSO_4$ and filtered. Solvent was removed by rotary evaporation to yield an off white solid, 487 mg (yield 95%). ^{1}H NMR (500 MHz, $CDCl_3$) δ 11.34 (s, 1H), 8.16 (d, *J* = 1.6 Hz, 1H), 8.12 – 8.04 (m, 2H), 7.95 – 7.88 (m, 3H), 7.82 (d, *J* = 7.9 Hz, 1H), 7.77 (d, *J* = 8.1 Hz, 1H), 7.66 – 7.60 (m, 3H), 7.51 (ddd, *J* = 8.3, 7.1, 1.2 Hz, 1H), 7.47 – 7.37 (m, 5H), 2.32 – 2.15 (m, 4H), 0.35 (t, *J* = 7.2 Hz, 6H).

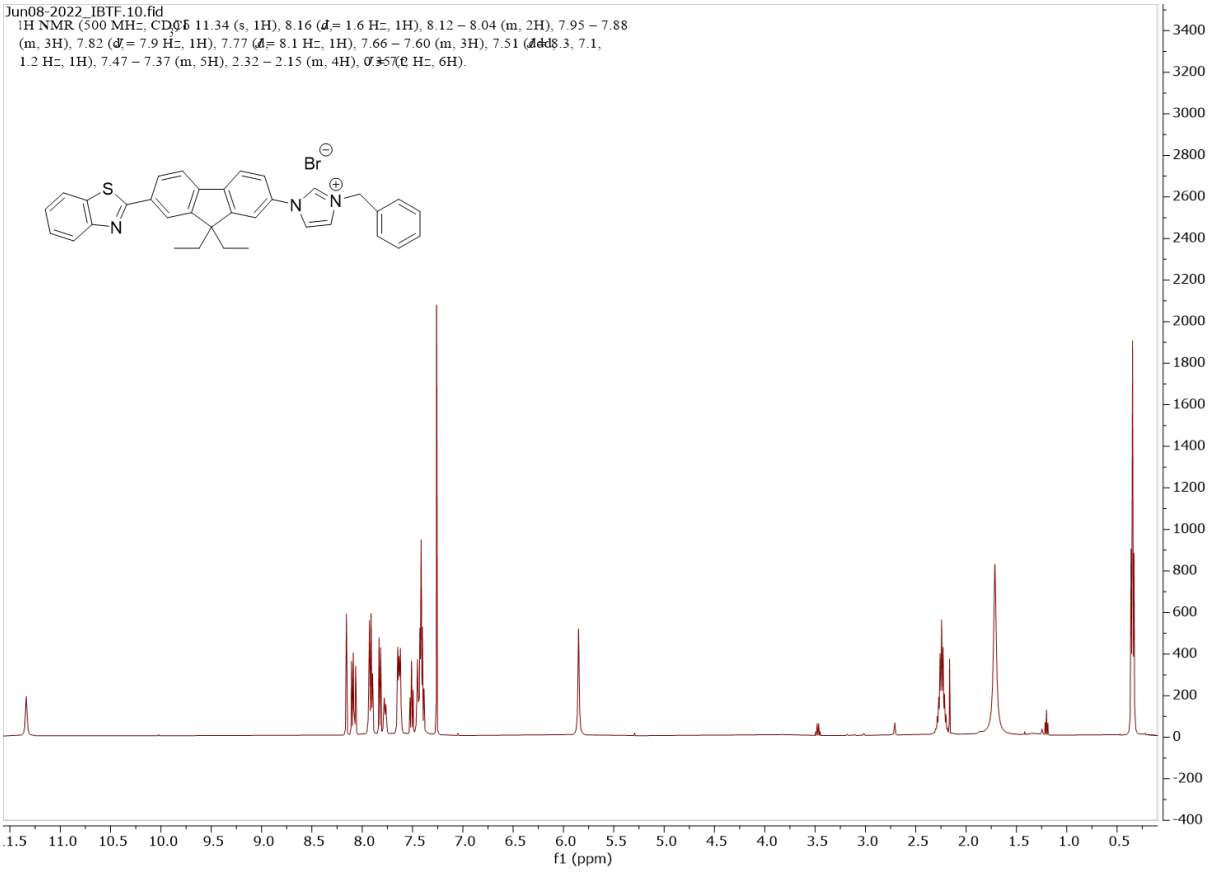

Figure S7: ^{1}H NMR of IBTF collected in d-chloroform.

3-benzyl-1-(7-(diphenylamino)-9,9-diethyl-9H-fluoren-2-yl)-1H-imidazol-3-ium (IDPA)

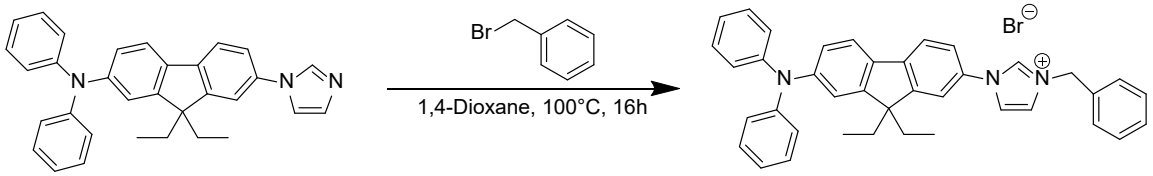

Scheme S2: Synthetic route for the attachment of the benzyl moiety to the imidazole of DPA-Im.

To a 50-mL round-bottom flask equipped with a Vigreux column was added DPA-Im (426 mg, 1.00 mmol) and benzyl bromide (0.218 mL, 1.84 mmol). The resulting solution was dissolved in 10 mL 1,4-dioxanewith stirring at 100°C for 16 h. The mixture was cooled to room temperature, whereupon 50 mL of deionized water was added to produce a light brown precipitate. The precipitate was filtered and washed with water (5 x 10 mL) and then redissolved in dichloromethane. The solution was dried with $MgSO_4$ and filtered. Solvent removal by rotary evaporation to yield 476 mg of a brown solid (yield 87%). ^{1}H NMR (500 MHz, $CDCl_3$) δ 11.27 (s, 1H), 7.77 (d, *J* = 2.2 Hz, 1H), 7.75 – 7.53 (m, 7H), 7.47 – 7.35 (m, 4H), 7.30 – 7.22 (m, 6H), 7.15 – 6.98 (m, 9H), 5.85 (s, 2H), 2.08 (dq, *J* = 14.5, 7.3 Hz, 2H), 1.98 – 1.86 (m, 3H), 0.36 (t, *J* = 14.7, 7.3 Hz, 6H).

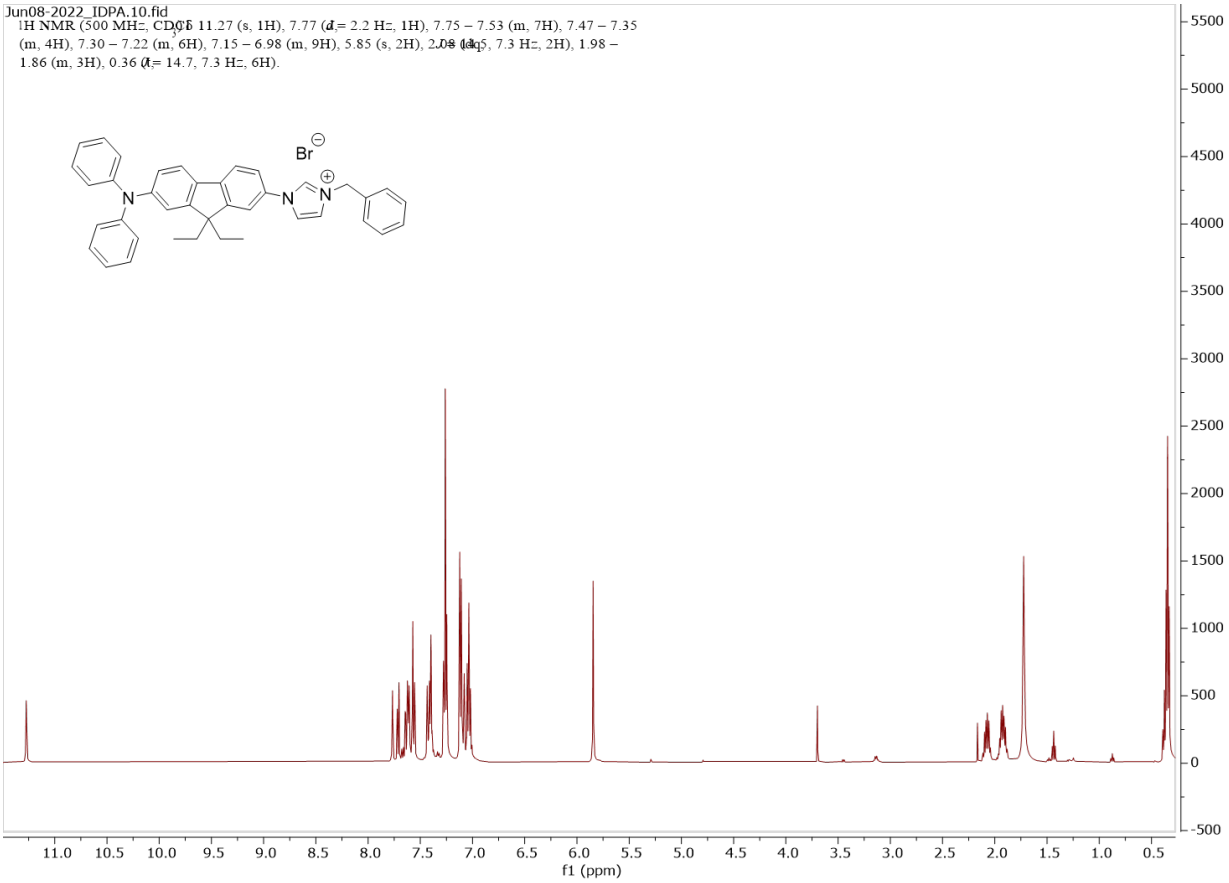

Figure S8: ^{1}H NMR of IDPA collected in d-chloroform.

(1-(7-(benzo[d]thiazol-2-yl)-9,9-diethyl-9H-fluoren-2-yl)-3-benzyl-1H-3l4-imidazol-2-yl)gold(I) bromide (IBTF-AuBr)

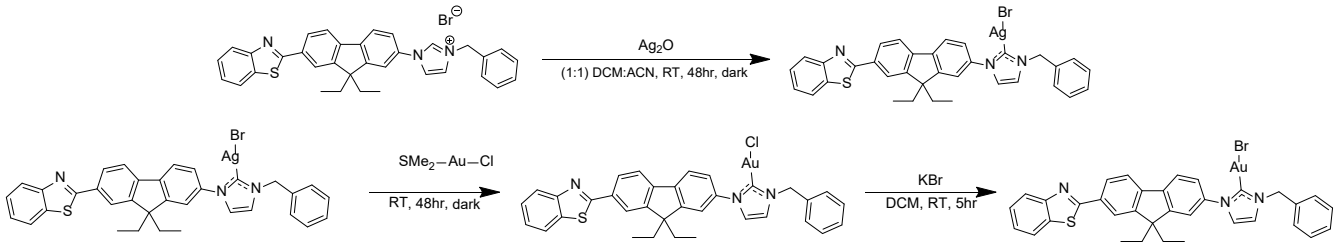

Scheme S3: Transmetalation of IBTF with Ag_2O and dimethylsulfide gold(I) chloride, followed by a halogen exchange with KBr.

Manipulations were performed on an argon Schlenk like with exclusion of air. To a flame-dried 250-mL round-bottom flask was added BTF-Im (625 mg, 1.06 mmol), which was dissolved in 60 mL anhydrous 1:1 (v/v) dichloromethane:acetonitrile. Ag_2O (123 mg, 0.53 mmol) was added, and the mixture was stirred in the absence of light at room temperature for 48 h under argon flow. Me_2SAuCl (312 mg, 1.06 mmol) was added with stirring in the absence of light or an additional 48 hrs. under argon flow. The brown/violet solution was filtered through Celite and the filtrate was evaporated to dryness. The pale-yellow solid was dissolved in dichloromethane and n-pentane was added with formation of a precipitate. The suspension was filtered and washed with n-pentane. The resulting solid was added to 20 mL of a 1:1 solution of dichloromethane:deionized water and KBr (284 mg, 2.4 mmol). The mixture was stirred for 5 h at room temperature. The organic layer was dried with $MgSO_4$ and solvent was removed by rotary evaporation affording 361 mg of a pale yellow solid (46% based on Me_2SAuCl). ^{1}H NMR (500 MHz, $CDCl_3$) δ 8.16 (d, *J* = 1.5 Hz, 1H), 8.13 – 8.05 (m, 2H), 7.93 (dt, *J* = 7.9, 0.9 Hz, 1H), 7.90 – 7.80 (m, 3H), 7.58 – 7.48 (m, 2H), 7.48 – 7.35 (m, 6H), 7.31 (d, *J* = 1.9 Hz, 1H), 7.07 (d, *J* = 2.0 Hz, 1H), 5.52 (s, 2H), 2.28 – 2.13 (m, 4H), 0.41 (t, *J* = 7.3 Hz, 6H). ^{13}C NMR (126 MHz, $CDCl_3$) δ 174.37, 168.37, 154.19, 152.59, 151.37, 142.94, 141.49, 138.42, 135.04, 133.14, 129.24, 128.35, 127.40, 126.43, 125.25, 123.26, 122.03, 121.81, 121.09, 120.73, 57.21, 32.67, 8.83. HRMS (FT-ESI, $[M+H]^+$) m/z calculated M+H 788.1004, measured M+H 788.0996.

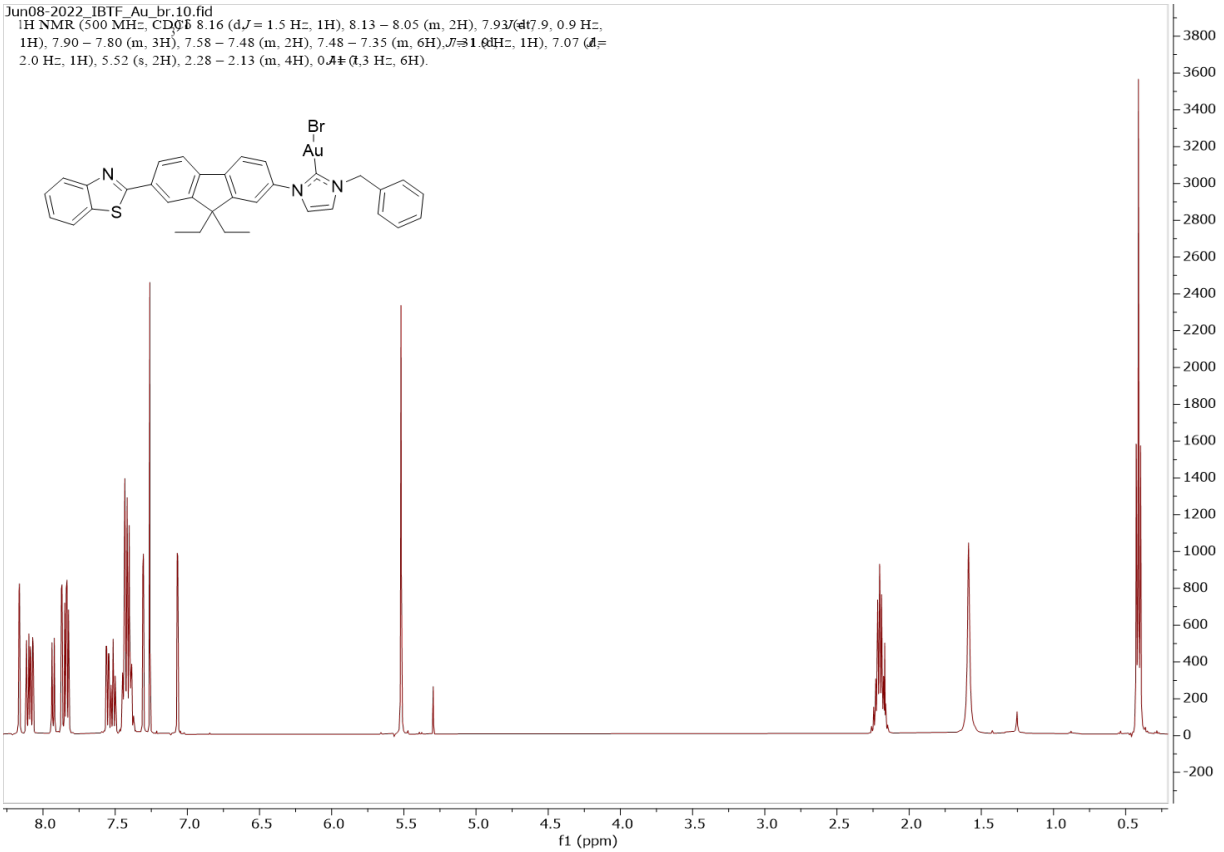

Figure S9: ^{1}H NMR of **IBTF-AuBr** collected in d-chloroform.

(3-benzyl-1-(7-(diphenylamino)-9,9-diethyl-9H-fluoren-2-yl)-1H-3l4-imidazol-2-yl)gold(II) bromide (IDAP-AuBr)

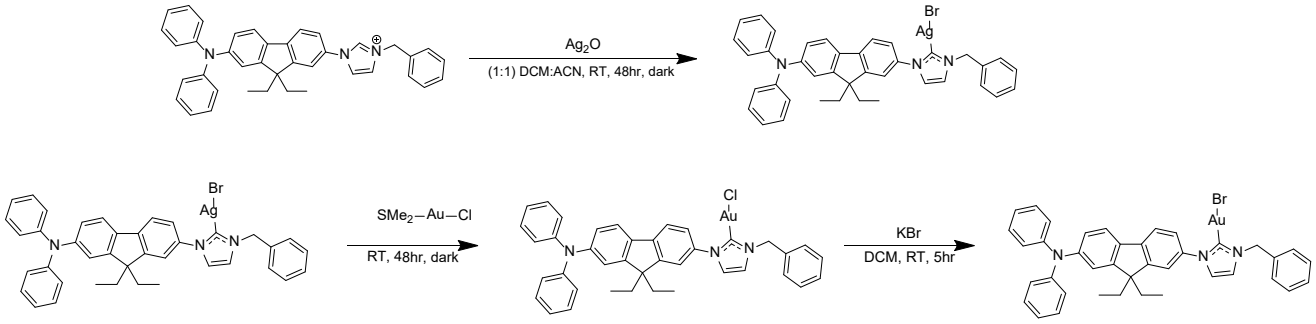

Scheme S4: Transmetalation of IDPA with Ag_2O and dimethylsulfide gold(I) chloride, followed by a halogen exchange with KBr.

Manipulations were performed under an argon atmosphere. To a flame-dried 250-mL round-bottom flask was added DPA-Im (542 mg, 1.06 mmol) and 60 mL of an anhydrous 1:1 dichloromethane:acetonitrile mixture. Ag_2O (123 mg, 0.53 mmol) was then added with stirring in the absence of light at room temperature for 48 h. To this suspension was added Me_2SAuCl (312 mg, 1.06 mmol) with stirring in the absence of light for an additional 48 h. The resulting brown/violet solution was filtered through Celite and the filtrate was evaporated to dryness under reduced pressure. The resulting pale-yellow solid was dissolved in dichloromethane and n-pentane was added to precipitate the product. The resulting suspension was then filtered and washed with n-pentane to provide 289 mg (crude yield 35%), which was then added to 20 mL of a 1:1 (v/v) mixture of dichloromethane: deionized water and KBr (218 mg, 1.83 mmol). This mixture was stirred for 5 h. The organic layer was dried with $MgSO_4$ and solvent was removed by rotary evaporation to afford a pale yellow solid (293 mg, 37% based on Me_2SAuCl). ^{1}H NMR (500 MHz, $CDCl_3$) δ 7.76 (s, 1H), 7.66 (d, *J* = 8.0 Hz, 1H), 7.57 (d, *J* = 8.2 Hz, 1H), 7.26 (t, *J* = 7.0 Hz, 7H), 7.15 – 7.08 (m, 5H), 7.07 – 6.99 (m, 4H), 5.52 – 5.49 (m, 2H), 2.02 (s, 1H), 1.91 (dq, *J* = 13.4, 7.0 Hz, 2H), 0.40 (t, *J* = 7.2 Hz, 6H). ^{13}C NMR (126 MHz, CDCl3) δ 174.22, 151.84, 151.72, 148.04, 142.38, 136.94, 134.79, 129.20, 128.32, 124.16, 123.30, 122.83, 122.11, 120.51, 119.45, 118.87, 56.66, 55.56, 32.56, 8.79. HRMS (FT-ESI, $[M+H]^+$) m/z calculated M+Na 844.1572, measured M+Na 844.1565.

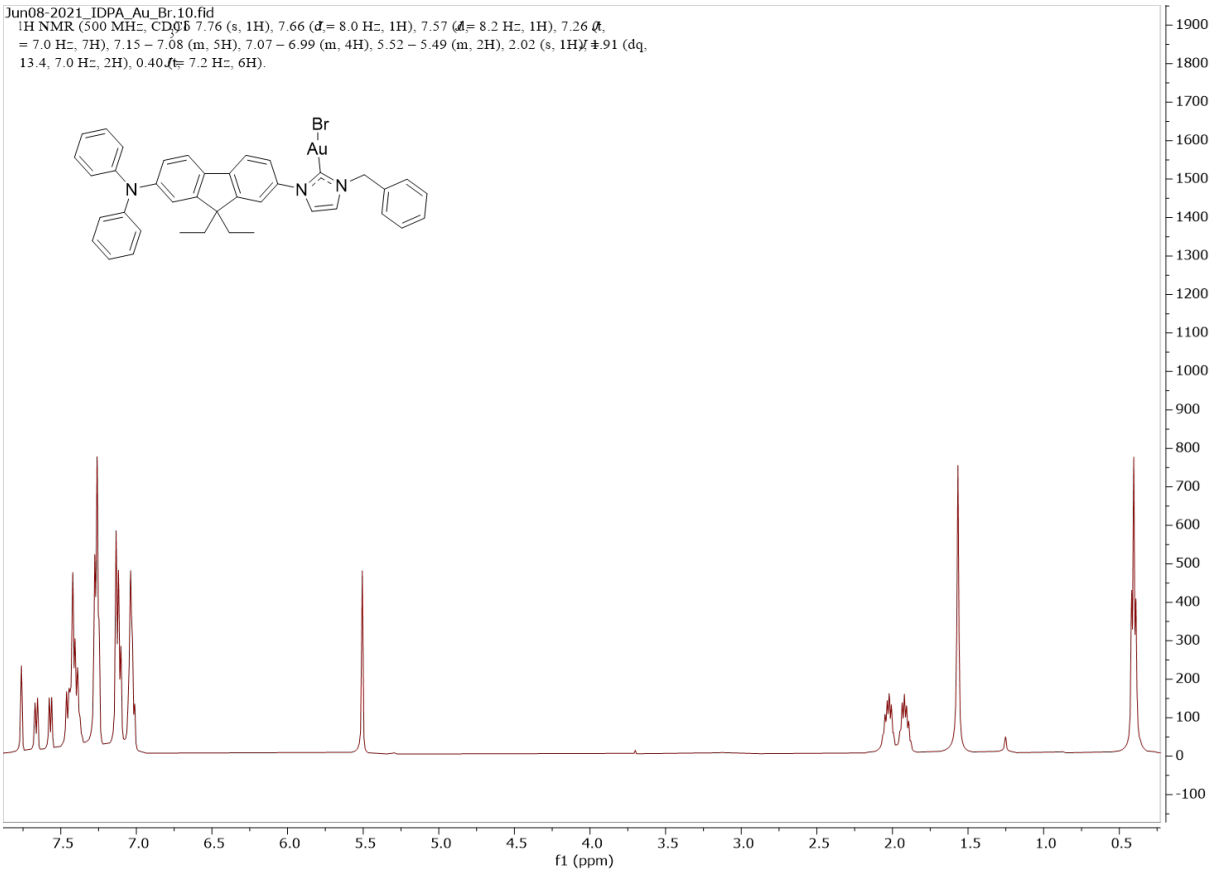

Figure S10: ^{1}H NMR of **IDPA-AuBr** collected in d-chloroform.

X-Ray Crystallography

Table S1. X-Ray Crystallographic Data for **IDPA-AuBr**.

	IDPA-AuBr
Crystal data	
Chemical formula	**$C_{39}H_{35}AuBrN_3$**
M_r	**822.57**
Crystal system, space group	**Triclinic, $P\bar{1}$**
Temperature (K)	**150**
a, b, c (Å)	**8.9870 (4), 12.5073 (6), 14.6318 (6)**
α, β, γ (°)	**88.091 (2), 86.564 (2), 84.418 (2)**
V (Å^3)	**1633.29 (13)**
Z	**2**
Radiation type	**Mo $K\alpha$**
μ (mm^{-1})	**5.76**
Crystal size (mm)	**0.33 × 0.29 × 0.18**
Data collection	
Diffractometer	**Bruker AXS D8 Quest**
Absorption correction	**Multi-scan *SADABS* 2016/2: Krause, L., Herbst-Irmer, R., Sheldrick G.M. & Stalke D., J. Appl. Cryst. 48 (2015) 3-10**
T_{min}, T_{max}	**0.432, 0.747**
No. of measured, independent and observed [$I > 2\sigma(I)$] reflections	**88451, 12493, 11279**
R_{int}	**0.049**
$(\sin \theta/\lambda)_{max}$ (Å^{-1})	**0.770**
Refinement	

$R[F^2 > 2\sigma F^2)]$, $wR(F^2)$, S	0.021, 0.051, 1.03
No. of reflections	12493
No. of parameters	399
H-atom treatment	H-atom parameters constrained
$\Delta\rangle_{max}$, $\Delta\rangle_{min}$ (e Å^{-3})	1.26, -1.26

Table S2. X-Ray Crystallographic Data for **IBTF-AuBr**.

	IBTF-AuBr
Crystal data	
Chemical formula	$C_{34}H_{29}AuBrN_3S$
M_r	788.54
Crystal system, space group	Monoclinic, $P2_1$
Temperature (K)	150
a, b, c (Å)	11.6803 (6), 10.7569 (6), 11.7494 (6)
β (°)	91.252 (3)
V (Å^3)	1475.89 (13)
Z	2
Radiation type	Cu $K\alpha$
μ (mm^{-1})	11.83
Crystal size (mm)	0.07 × 0.03 × 0.01
Data collection	
Diffractometer	Bruker AXS D8 Quest CMOS diffractometer with PhotonII charge-integrating pixel array detector (CPAD)
Absorption correction	Multi-scan *SADABS* 2016/2: Krause, L., Herbst-Irmer, R., Sheldrick G.M. & Stalke D., J. Appl. Cryst. 48 (2015) 3-10
T_{min}, T_{max}	0.135, 0.330

No. of measured, independent and observed [$I > 2\sigma(I)$] reflections	**13058, 5885, 5457**
R_{int}	**0.068**
$(\sin \theta/\lambda)_{max}$ (Å^{-1})	**0.641**
Refinement	
$R[F^2 > 2\sigma(F^2)]$, $wR(F^2)$, S	**0.047, 0.115, 1.02**
No. of reflections	**5885**
No. of parameters	**363**
No. of restraints	**1**
H-atom treatment	**H-atom parameters constrained**
$\Delta\rangle_{max}$, $\Delta\rangle_{min}$ (e Å^{-3})	**2.19, -0.84**
Absolute structure	**Flack x determined using 2141 quotients [(I+)-(I-)]/[(I+)+(I-)] (Parsons, Flack and Wagner, Acta Cryst. B69 (2013) 249-259).**
Absolute structure parameter	**-0.013 (9)**

Calculations. Spin-restricted density-functional theory computations were performed in Gaussian16 rev. A.03.[8] Geometries were optimized with the 6-31G(d) basis set for nonmetal atoms and the Stuttgart-Dresden effective core potential and basis set for Au; scalar relativistic effects are included implicitly.[9] Optimizations proceeded without constraints, and harmonic frequency calculations found all real vibrational frequencies, confirming that converged structures are local energy minima. Final single-point calculations employed the exchange and correlation functionals of Perdew, Burke, and Ernzerhof (PBE0),[10] and the TZVP basis set. Continuum solvation in toluene was imposed using the integral equation formalism of the polarizable continuum model.[11,12] Population analyses were performed with the AOMix-CDA program of Gorelsky.[13,14] Orbital depictions employ a contour level of 0.02 a.u.

Table S3. Calculated Bond dissociation Enthalpies of Au–C and Au-Br for **IDPA-AuBr'** and **IBTF-AuBr'**

Calculated gas-phase bond dissociation enthalpies (BDE) of model complexes at 298 K. The bond being broken appears in red.

Bond	BDE (kcal mol^{-1})	
IBTF-Au–Br'	140.8	(heterolytic)
IBTF-Au–Br'	104.4	(homolytic)
IDPA-Au–Br'	138.5	(heterolytic)
IDPA-Au–Br'	104.7	(homolytic)
IBTF–AuBr'	76.7	
IDPA–AuBr'	77.4	

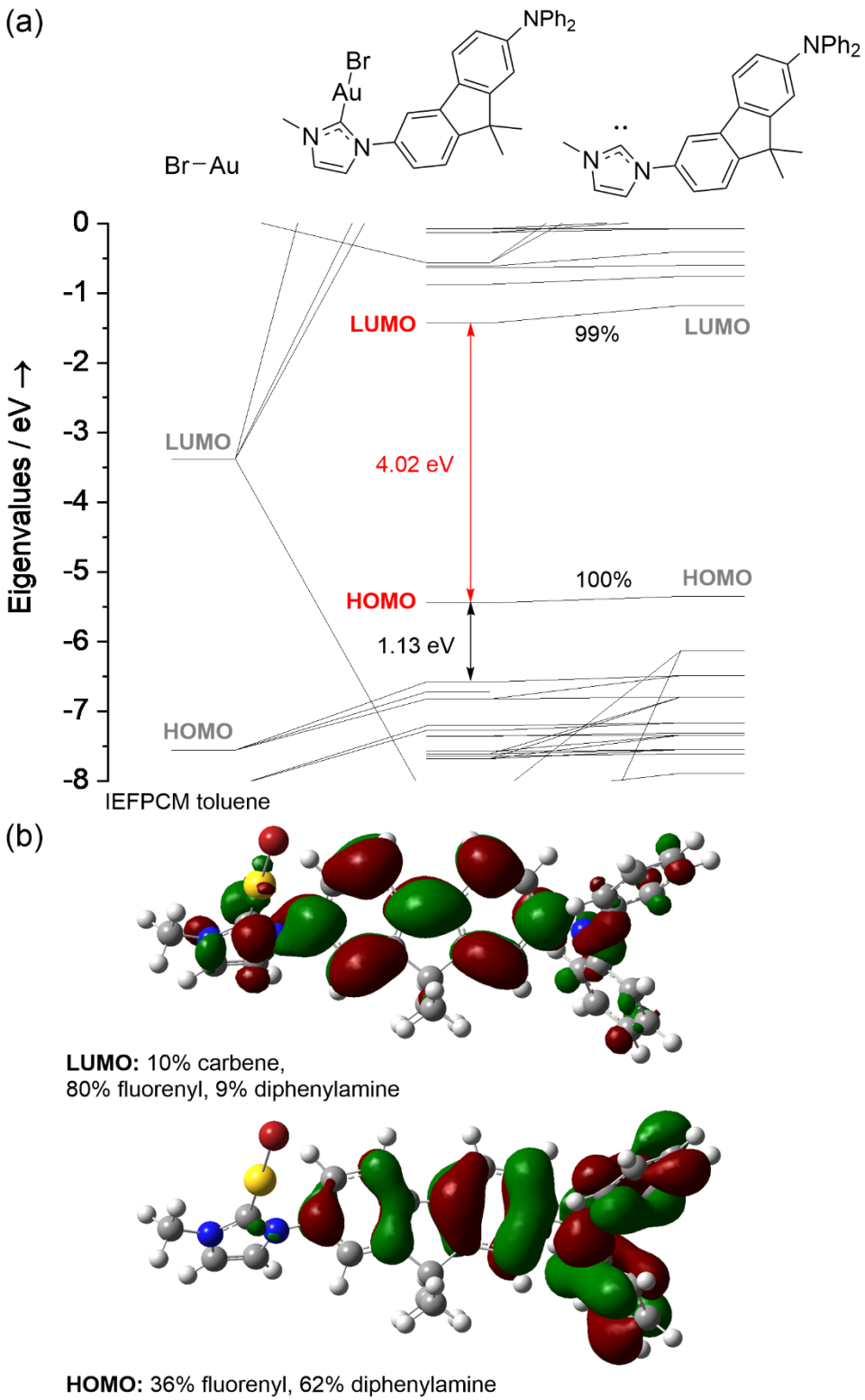

Figure S11: (a) Partial Kohn-Sham orbital energy level diagram of **IDPA-AuBr'** in continuum toluene. Percentages are of electron density. (b) Plots of selected orbitals. Contour level 0.02 a.u.

Table S3. Summary of calculated electronic transitions to Franck-Condon singlet states of **IDPA-AuBr2.** MO 144: HOMO; MO 145: LUMO

#	nm	1000 cm-1	eV	f	Assignment (excitations with contrib. > 10.0%)
1	373.1	26.80	3.323	0.8626	144->145(96.5%)
2	334.5	29.89	3.706	0.0345	144->146(87.5%)
3	314.6	31.79	3.941	0.2540	144->147(90.4%)
4	303.1	32.99	4.090	0.0135	144->148(71.7%)
5	285.1	35.08	4.349	0.0060	144->149(72.0%) 144->150(15.1%)
6	278.2	35.95	4.457	0.0505	144->150(54.5%) 144->151(20.0%) 144->149(12.3%)
7	275.4	36.31	4.503	0.1192	144->151(31.8%) 143->145(29.7%) 144->152(12.3%)
8	274.8	36.39	4.512	0.0516	143->145(58.4%) 144->151(20.2%)
9	265.8	37.62	4.664	0.0447	142->145(81.3%)
10	261.9	38.18	4.733	0.1317	141->145(73.6%)
11	258.3	38.71	4.800	0.0100	144->152(45.0%) 144->154(13.5%) 144->151(12.1%)
12	249.8	40.03	4.964	0.0431	143->146(22.4%) 140->145(19.9%) 141->146(13.4%) 139->145(10.1%)
13	247.4	40.42	5.012	0.0562	140->145(51.6%) 143->146(13.2%)
14	242.9	41.18	5.105	0.0301	139->145(45.4%)
15	242.2	41.30	5.120	0.0065	144->154(47.8%) 144->153(19.3%) 144->152(10.5%)
16	239.8	41.69	5.169	0.0090	144->153(50.9%) 144->154(14.1%)
17	239.0	41.83	5.187	0.0849	143->149(53.1%)
18	238.6	41.91	5.196	0.0025	143->146(20.8%) 141->146(17.2%) 144->153(11.7%)
19	237.0	42.19	5.231	0.0466	142->149(54.0%) 142->148(14.4%)
20	234.8	42.58	5.279	0.0200	137->145(16.9%) 139->145(11.5%) 141->148(10.0%)

Table S4. Summary of calculated electronic transitions to Franck-Condon triplet states of **IDPA-AuBr2.** MO 144: HOMO; MO 145: LUMO

#	nm	1000 cm-1	eV	f	Assignment (excitations with contrib. > 10.0%)
1	489.8	20.41	2.531	0.0000	144->145(72.4%)
2	405.9	24.64	3.055	0.0000	144->147(66.8%)
3	373.1	26.80	3.323	0.0000	144->146(79.1%)
4	368.2	27.16	3.368	0.0000	141->145(16.9%)
5	337.4	29.64	3.675	0.0000	144->148(51.1%)
6	330.1	30.29	3.756	0.0000	

Table S5. Summary of calculated electronic transitions to Franck-Condon singlet states of **IBTF-AuBr2.** MO 134: HOMO; MO 135: LUMO

#	nm	1000 cm-1	eV	f	Assignment (excitations with contrib. > 10.0%)
1	352.6	28.36	3.516	1.5836	134->135(97.9%)
2	303.9	32.90	4.080	0.0183	133->135(95.8%)
3	300.8	33.24	4.122	0.0346	131->135(90.5%)
4	295.3	33.86	4.198	0.0040	132->135(95.3%)
5	284.2	35.18	4.362	0.0063	134->136(34.8%) 128->135(24.0%) 134->137(10.2%)
6	276.4	36.18	4.486	0.0305	130->135(61.5%) 128->135(17.9%)
7	271.2	36.87	4.572	0.0029	129->135(40.1%) 134->136(17.1%) 130->135(16.9%)
8	262.6	38.08	4.721	0.0145	134->137(51.5%) 134->136(13.5%) 129->135(13.1%)
9	261.3	38.27	4.745	0.0436	129->135(29.4%) 128->135(28.0%) 134->136(22.1%)
10	258.4	38.69	4.798	0.0002	125->135(91.9%)

11	248.5	40.25	4.990	0.0426	127->135(40.5%) 134->139(12.9%) 134->137(11.1%)
12	247.3	40.44	5.013	0.1113	133->136(44.4%)
13	247.0	40.48	5.019	0.0134	132->136(44.1%) 132->138(19.4%) 132->137(13.6%)
14	245.2	40.78	5.056	0.0062	134->139(40.2%)
15	243.5	41.08	5.093	0.0041	126->135(33.6%) 133->137(26.1%) 127->135(20.4%)
16	242.5	41.23	5.112	0.0320	133->137(39.2%) 126->135(26.2%)
17	239.4	41.77	5.179	0.0156	134->138(57.1%)
18	236.7	42.24	5.238	0.0441	132->137(61.7%) 132->136(29.8%)
19	232.0	43.11	5.345	0.0614	134->140(35.4%) 131->136(27.6%) 134->139(14.4%)
20	231.2	43.25	5.363	0.0387	130->136(27.8%) 134->138(12.0%)

Table S6. Summary of calculated electronic transitions to Franck-Condon triplet states of **IBTF-AuBr2.** MO 134: HOMO; MO 135: LUMO

#	nm	1000 cm-1	eV	f	Assignment (excitations with contrib. > 10.0%)
1	514.6	19.43	2.409	0.0000	134->135(82.0%)
2	395.9	25.26	3.132	0.0000	131->135(21.1%) 129->135(12.5%) 134->136(11.0%) 130->135(10.9%)
3	351.7	28.44	3.526	0.0000	131->135(42.0%)
4	329.4	30.36	3.764	0.0000	128->135(21.4%) 131->135(13.9%)
5	317.9	31.46	3.900	0.0000	128->135(31.3%) 129->135(11.2%)
6	313.4	31.91	3.956	0.0000	134->136(22.4%) 134->137(18.7%) 128->135(11.8%) 133->135(10.4%)

Table S7. Optimized Cartesian coordinates (Å) of **IDPA-AuBr2.**

Au	0.204197	4.152296	0.392660
Br	-0.235201	6.528919	0.561412
C	0.237961	-0.049344	0.221188
C	1.568789	0.175862	0.117245
N	1.741026	1.547328	0.138273
C	0.544452	2.181588	0.261799
N	-0.369183	1.185340	0.305201
H	-0.325142	-0.969829	0.234248
H	2.399844	-0.502483	0.004357
C	-1.801878	1.373799	0.437868
H	-2.003966	2.444531	0.481132
H	-2.315455	0.940019	-0.424056
H	-2.157478	0.898472	1.355669
C	3.014657	2.184659	0.056316
C	3.230144	3.188152	-0.889066
C	4.031829	1.765704	0.917895
C	4.475051	3.804087	-0.974378
H	2.423722	3.478859	-1.554840
C	5.273580	2.370496	0.819048
H	3.831178	0.994616	1.658059
C	5.497865	3.392310	-0.121550
H	4.636703	4.590209	-1.706443
C	6.525066	2.096513	1.636004
C	6.879745	3.843426	0.011556
C	7.495888	3.097010	1.029514
C	7.601504	4.824619	-0.666427
C	8.814872	3.325022	1.379914
C	8.930537	5.044977	-0.329788
H	7.144147	5.408446	-1.461096

C	9.549609	4.306656	0.694060
H	9.290475	2.761651	2.178172
H	9.507128	5.795729	-0.861070
C	6.290666	2.376519	3.127517
H	5.542698	1.687822	3.536705
H	7.219481	2.240062	3.692744
H	5.938212	3.400602	3.285217
C	7.016177	0.654987	1.438548
H	6.282341	-0.059936	1.828567
H	7.182129	0.436281	0.378735
H	7.958884	0.495484	1.973957
N	10.896190	4.549839	1.028751
C	11.402258	5.870899	1.026890
C	10.640222	6.925220	1.545723
C	12.675325	6.140253	0.509230
C	11.141222	8.222340	1.535027
H	9.655498	6.721116	1.955671
C	13.175149	7.437844	0.519794
H	13.267871	5.327017	0.100665
C	12.411654	8.487408	1.027246
H	10.536768	9.029041	1.941172
H	14.164997	7.629866	0.114192
H	12.802401	9.500873	1.027214
C	11.745996	3.476494	1.382081
C	11.702013	2.270736	0.670234
C	12.647513	3.605938	2.446107
C	12.535903	1.216368	1.025690
H	11.011934	2.167916	-0.162035
C	13.490066	2.552051	2.782621
H	12.682924	4.536627	3.004527
C	13.437690	1.349810	2.079921
H	12.489754	0.288399	0.461716
H	14.183644	2.669663	3.611064
H	14.093052	0.526708	2.349783

Table S8. Optimized Cartesian coordinates (Å) of **IBTF-AuBr2.**

Au	0.408125	4.069440	-0.491581
Br	0.059163	6.418667	-0.965260
C	0.273251	-0.048082	0.352725
C	1.612401	0.136046	0.422299
N	1.842805	1.470319	0.142079
C	0.672621	2.123587	-0.091785
N	-0.281086	1.173904	0.036351
H	-0.327112	-0.934216	0.490284
H	2.417608	-0.555224	0.615506
C	-1.706438	1.398074	-0.120061
H	-1.863394	2.449719	-0.361937
H	-2.094094	0.775332	-0.930449
H	-2.226024	1.156567	0.810658
C	3.140181	2.061507	0.125074
C	3.546806	2.810418	-0.980898
C	3.986133	1.853277	1.216491
C	4.814910	3.381258	-1.000859
H	2.870342	2.937607	-1.819888
C	5.253877	2.411624	1.186494
H	3.635320	1.281840	2.072398

C	5.667435	3.177967	0.082855
H	5.126979	3.968795	-1.859481
C	6.344893	2.333686	2.240289
C	7.030759	3.639669	0.330344
C	7.443416	3.153352	1.583949
C	7.886859	4.423083	-0.441129
C	8.704247	3.442589	2.069301
C	9.154152	4.712639	0.048444
H	7.577469	4.807022	-1.409201
C	9.575706	4.230398	1.297290
H	9.047716	3.080933	3.034041
H	9.823549	5.323091	-0.552537
C	5.890977	2.969265	3.562877
H	5.058945	2.403170	3.996701
H	6.712962	2.969856	4.287217
H	5.563411	4.002587	3.412266
C	6.792925	0.883621	2.475364
H	5.972054	0.289686	2.893605
H	7.119450	0.414010	1.542004
H	7.626351	0.852033	3.185736
C	10.907296	4.524390	1.828159
S	12.050485	5.540368	0.937716
N	11.342051	4.075462	2.965957
C	13.196798	5.324921	2.224448
C	12.622892	4.504235	3.221762
C	14.488920	5.832676	2.349939
C	13.366602	4.189674	4.366665
C	15.207572	5.507940	3.493393
H	14.922664	6.463056	1.579789
C	14.651073	4.693882	4.492038
H	12.924217	3.559326	5.131898
H	16.216479	5.891877	3.614422
H	15.237153	4.457171	5.375422

SI References

(1) Suzuki, K.; Kobayashi, A.; Kaneko, S.; Takehira, K.; Yoshihara, T.; Ishida, H.; Shiina, Y.; Oishi, S.; Tobita, S. Reevaluation of Absolute Luminescence Quantum Yields of Standard Solutions Using a Spectrometer with an Integrating Sphere and a Back-Thinned CCD Detector. *Physical Chemistry Chemical Physics* **2009**, *11* (42), 9850–9860. https://doi.org/10.1039/B912178A.

(2) Mihaly, J. J.; Wolf, S. M.; Phillips, A. T.; Mam, S.; Yung, Z.; Haley, J. E.; Zeller, M.; de La Harpe, K.; Holt, E.; Grusenmeyer, T. A.; Collins, S.; Gray, T. G. Synthetically Tunable White-, Green-, and Yellow-Green-Light Emission in Dual-Luminescent Gold(I) Complexes Bearing a Diphenylamino-2,7-Fluorenyl Moiety. *Inorganic Chemistry* **2022**, *61* (3), 1228–1235. https://doi.org/10.1021/acs.inorgchem.1c02405.

(3) Cekli, S.; Winkel, R. W.; Alarousu, E.; Mohammed, O. F.; Schanze, K. S. Triplet Excited State Properties in Variable Gap π-Conjugated Donor–Acceptor–Donor Chromophores. *Chemical Science* **2016**, *7* (6), 3621–3631. https://doi.org/10.1039/C5SC04578A.

(4) Wilkinson, F.; Helman, W. P.; Ross, A. B. Quantum Yields for the Photosensitized Formation of the Lowest Electronically Excited Singlet State of Molecular Oxygen in Solution. *Journal of Physical and Chemical Reference Data* **1993**, *22* (1), 113–262. https://doi.org/10.1063/1.555934.

(5) Resch-Genger, U.; Rurack, K. Determination of the Photoluminescence Quantum Yield of Dilute Dye Solutions (IUPAC Technical Report). *Pure and Applied Chemistry* **2013**, *85* (10), 2005–2013. https://doi.org/10.1351/pac-rep-12-03-03.

(6) de Frémont, P.; Singh, R.; Stevens, E. D.; Petersen, J. L.; Nolan, S. P. Synthesis, Characterization and Reactivity of N-Heterocyclic Carbene Gold(III) Complexes. *Organometallics* **2007**, *26* (6), 1376–1385. https://doi.org/10.1021/om060887t.

(7) Kannan, R.; He, G. S.; Yuan, L.; Xu, F.; Prasad, P. N.; Dombroskie, A. G.; Reinhardt, B. A.; Baur, J. W.; Vaia, R. A.; Tan, L.-S. Diphenylaminofluorene-Based Two-Photon-Absorbing Chromophores with Various π-Electron Acceptors. *Chem. Mater.* **2001**, *13* (5), 1896–1904. https://doi.org/10.1021/cm000747o.

(8) Frisch, M. J.; Trucks, G. W.; Schlegel, H. B.; Scuseria, G. E.; Robb, M. A.; Cheeseman, J. R.; Scalmani, G.; Barone, V.; Petersson, G. A.; Nakatsuji, H.; Li, X.; Caricato, M.; Marenich, A. V.; Bloino, J.; Janesko, B. G.; Gomperts, R.; Mennucci, B.; Hratchian, H. P.; Ortiz, J. V.; Izmaylov, A. F.; Sonnenberg, J. L.; Williams-Young, D.; Ding, F.; Lipparini, F.; Egidi, F.; Goings, J.; Peng, B.; Petrone, A.; Henderson, T.; Ranasinghe, D.; Zakrzewski, V. G.; Gao, J.; Rega, N.; Zheng, G.; Liang, W.; Hada, M.; Ehara, M.; Toyota, K.; Fukuda, R.; Hasegawa, J.; Ishida, M.; Nakajima, T.; Honda, Y.; Kitao, O.; Nakai, H.; Vreven, T.; Throssell, K.; Montgomery Jr., J. A.; Peralta, J. E.; Ogliaro, F.; Bearpark, M. J.; Heyd, J. J.; Brothers, E. N.; Kudin, K. N.; Staroverov, V. N.; Keith, T. A.; Kobayashi, R.; Normand, J.; Raghavachari, K.; Rendell, A. P.; Burant, J. C.; Iyengar, S. S.; Tomasi, J.; Cossi, M.; Millam, J. M.; Klene, M.; Adamo, C.; Cammi, R.; Ochterski, J. W.; Martin, R. L.; Morokuma, K.; Farkas, O.; Foresman, J. B.; Fox, D. J. Gaussian 16, Revision A.03, 2016.

(9) Dolg, M.; Wedig, U.; Stoll, H.; Preuss, H. Energy-adjusted Ab Initio Pseudopotentials for the First Row Transition Elements. *The Journal of Chemical Physics* **1987**, *86* (2), 866–872. https://doi.org/10.1063/1.452288.

(10) Perdew, J. P.; Burke, K.; Ernzerhof, M. Generalized Gradient Approximation Made Simple. *Physical Review Letters* **1996**, *77* (18), 3865–3868. https://doi.org/10.1103/PhysRevLett.77.3865.

(11) Miertuš, S.; Scrocco, E.; Tomasi, J. Electrostatic Interaction of a Solute with a Continuum. A Direct Utilizaion of AB Initio Molecular Potentials for the Prevision of Solvent Effects. *Chemical Physics* **1981**, *55* (1), 117–129. https://doi.org/10.1016/0301-0104(81)85090-2.

(12) Cancès, E.; Mennucci, B.; Tomasi, J. A New Integral Equation Formalism for the Polarizable Continuum Model: Theoretical Background and Applications to Isotropic and Anisotropic Dielectrics. *The Journal of Chemical Physics* **1997**, *107* (8), 3032–3041. https://doi.org/10.1063/1.474659.
(13) Gorelsky, S. I. *AOMix: Program for Molecular Orbital Analysis*. http://www.sg-chem.net.
(14) Gorelsky, S. I.; Lever, A. B. P. Electronic Structure and Spectra of Ruthenium Diimine Complexes by Density Functional Theory and INDO/S. Comparison of the Two Methods. *Journal of Organometallic Chemistry* **2001**, *635* (1), 187–196. https://doi.org/10.1016/S0022-328X(01)01079-8.